HIGH RESOLUTION MILLIMETRE IMAGING OF THE CI TAU PROTOPLANETARY DISC - A MASSIVE ENSEMBLE OF PROTOPLANETS FROM 0.1 - 100 AU

C. J. Clarke,[1] M. Tazzari,[1] A. Juhasz,[1] G. Rosotti,[1] R. Booth,[1] S. Facchini,[2] J.D. Ilee,[1] C.M. Johns-Krull,[3] M. Kama,[1] F. Meru,[1,4,5] and L. Prato[6]

[1]*Institute of Astronomy, Madingley Road, Cambridge, CB3 OHA, UK*

[2]*Max-Planck-Institut für Extratterristische Physik, Giessenbachstrasse 1, 85748 Garching, DE*

[3]*Physics & Astronomy Dept., Rice University, 6100 Main St., Houston, TX 77005, USA*

[4]*Department of Physics, University of Warwick, Gibbet Hill Road, Coventry,CV4 7AL, UK*

[5]*Centre for Exoplanets and Habitability, University of Warwick, Gibbet Hill Road, Coventry, CV4 7AL, UK*

[6]*Lowell Observatory, 1400 West Mars Hill Road, Flagstaff, AZ 86001 USA*

ABSTRACT

We present high resolution millimeter continuum imaging of the disc surrounding the young star CI Tau, a system hosting the first hot Jupiter candidate in a protoplanetary disc system. The system has extended mm emission on which are superposed three prominent annular gaps at radii ∼ 13, 39 and 100 au. We argue that these gaps are most likely to be generated by massive planets so that, including the hot Jupiter, the system contains four gas giant planets at an age of only 2 Myr. Two of the new planets are similarly located to those inferred in the famous HL Tau protoplanetary disc; in CI Tau, additional observational data enables a more complete analysis of the system properties than was possible for HL Tau. Our dust and gas dynamical modeling satisfies every available observational constraint and points to the most massive ensemble of exo-planets ever detected at this age, with its four planets spanning a factor 1000 in orbital radius.Our results show that the association between hot Jupiters and gas giants on wider orbits, observed in older stars, is apparently in place at an early evolutionary stage.

1. INTRODUCTION

Since the 1995 discovery of the first hot Jupiter (Mayor & Queloz 1995), it is now established that such gas giant planets orbiting at radii < 0.1 au from their parent stars are found in around 1% of main sequence solar type stars (Wright et al. 2012). There is considerable debate as to whether these objects formed *in situ* or have instead migrated from larger radii, either from interaction with their natal protoplanetary disc (Kley & Nelson 2012) or planet-planet scattering after the disc has dispersed (Rasio & Ford 1996). With typical ages of up to several Gyr, most hot Jupiter hosts have long since lost their protoplanetary discs (typical lifetime of a few Myr; Haisch et al. (2001)); arguments about the origin of hot Jupiters are thus usually based on theoretical models linking hypothetical initial conditions to present day orbital parameters. The recent discovery (Johns-Krull et al. 2016; Bid-

dle et al. 2018), using the radial velocity technique, of a hot Jupiter in the young disc bearing solar type star CI Tau, has demonstrated that in at least this case the hot Jupiter is already in a very close orbit when the star is only ∼ 2 Myr old (Guilloteau et al. 2014). CI Tau is a well studied system, with mass $0.92 M_\odot$ (Simon et al. 2017), luminosity $0.93 L_\odot$ (Guilloteau et al. 2014), and is already known to host a massive dust and gas disc extending many hundreds of au from the star (Guilloteau et al. 2011; Andrews & Williams 2007); additionally it displays a high accretion rate of gas onto the star (McClure et al. 2013). The hot Jupiter's mass is ∼ 11.3 M_{Jupiter} if its orbit is aligned with the outer disc (Guilloteau et al. 2014), consistent with the orbital alignment between hot Jupiters and outer planets found in mature exo-planetary systems (Becker et al. 2017). This mass places it in the top 5 % of the main sequence hot Jupiter population. Around half of *mature* hot Jupiter systems also contain companions (Knutson et al. 2014; Ngo et al. 2015) at less than 20 au which, if present at early times, would create structure in the protoplanetary disc. Although previous sub-millimetre

Corresponding author: Cathie Clarke

cclarke@ast.cam.ac.uk

observations have hinted at a possible gap in the disc around CI Tau at 100 au, they lacked the resolution to characterise this in detail or probe the inner disc where companions may be expected (Konishi et al. 2018). Here we present high resolution 1.3mm ALMA imaging of the disc surrounding CI Tau and report three pronounced annular gaps in emission between 10 and 100 AU. We present visibility modeling and explore the origin of these structures via hydrodynamical modeling, arguing for the presence of three gas giants as outer companions to the hot Jupiter.

2. OBSERVATIONS

CI Tau was observed with the Atacama Large Millimeter Array (ALMA) on the 23rd and 24th September 2017 (Project ID: 2016.1.01370.S, PI: Clarke) with 40 antennas (baselines between 21 and 12145.2 m) and an on-source integration time of 32.35 min in both cases. The correlator used four spectral windows centered at 224, 226, 240, and 242 GHz in time division mode to measure the continuum in Band 6. Each spectral window used 128 channels and a bandwidth of 1.875 GHz, together providing an effective total continuum bandwidth of 7.5 GHz. To calibrate the visibilities a set of standard calibrators were also observed. Calibration of the complex interferometric visibilities used the Common Astronomy Software Applications (CASA) v5.1.1 and the ALMA Pipeline. In panel (a) of Figure 1 we imaged the calibrated visibilities using the multi-scale CLEAN algorithm with scale parameters of 0", 0.048", 0.08", 0.24" and Briggs weighting with a robust parameter of 0.5 to obtain the optimal signal-to-noise ratio and spatial resolution. The resulting synthesized beam is 0.05" × 0.03" with a position angle of 16 degrees, while the achieved RMS noise level is 13μJy beam^{-1}.

3. VISIBILITY MODELLING

We characterise the CI Tau brightness by fitting the continuum visibilities with an axisymmetric parametric model consisting of an envelope and three gaps. For the envelope we use an exponentially-tapered power-law:

$$I_{\rm env}(R) = I_0 \left(\frac{R}{R_c}\right)^{\gamma_1} \exp\left[-\left(\frac{R}{R_c}\right)^{\gamma_2}\right] \quad \text{for} \quad R \leq R_{\rm out} \quad (1)$$

with I_0 a brightness normalisation constant (Jy sr^{-1}). Each gap is parametrised as the difference of two logistic functions:

$$I_{\rm gap}(R) = \delta_{\rm gap}\left[\frac{1}{1 + e^{-k_2(R-R_{\rm g}-w_2)}} - \frac{1}{1 + e^{-k_1(R-R_{\rm g}+w_1)}}\right], \quad (2)$$

where $\delta_{\rm gap}$ describes the gap depth ($\delta_{\rm gap} = 0$ corresponding to no gap), $R_{\rm g}$ is the gap radial location, w_1 and w_2 are the left- and right-hand gap widths at half depth and k_1, k_2 express

the steepness of the left and right gap profile. The brightness profile is given by:

$$I(R) = I_{\rm env}(1 + I_{\rm gap,1})(1 + I_{\rm gap,2})(1 + I_{\rm gap,3}), \quad (3)$$

involving 5 free parameters for $I_{\rm env}$ and 6 free parameters for each $I_{\rm gap}$. We simultaneously fit the disc inclination i and position angle PA (defined East of North) and the offset (ΔRA,ΔDec) from the phase center. We thus have a parameter set $\theta = (I_0, R_c, \gamma_1, \gamma_2, \ldots)$ described by 23 parameters for the brightness profile plus 4 for the system geometry. The computation of the visibilities $V_{\rm mod}$ for each model θ is performed using GALARIO[1] (Tazzari et al. 2018), which first computes the 2D image of the disc for a given $I(R)$ and then Fourier transforms and samples it in the observed (u, v) points. The likelihood of the observations $V_{\rm obs}$ given the model visibilities $V_{\rm mod}(\theta)$ is assumed Gaussian:

$$\log p(V_{\rm obs} \,|\, \theta) = -\frac{1}{2}\chi^2 = -\frac{1}{2}\sum_{j=1}^{N} |V_{\rm mod} - V_{\rm obs}|^2 w_j, \quad (4)$$

where N is the total number of visibility points and w_j is the weight[2] of the $j-$th visibility. The parameter space is explored with a Bayesian approach using the EMCEE Markov chain Monte Carlo (MCMC) ensemble sampler (Foreman-Mackey et al. 2013), providing an estimate of the posterior probability distribution of the model parameters given the observations:

$$\log p(\theta \,|\, V_{\rm obs}) = \log p(V_{\rm obs} \,|\, \theta) + \log p(\theta) + C, \quad (5)$$

where $p(\theta)$ is the prior on the parameters and C is a normalisation constant. Since the parameters are independent, the priors can be written as $p(\theta) = \prod_i p(\theta_i)$. We choose uniform priors on all parameters, except for inclination for which $p(i) = \sin(i)$ for $0 \leq i \leq \pi/2$. We run the MCMC sampler with 120 walkers for 50×10^3 steps after a burn in phase of 30×10^3 steps. We assessed convergence through visual inspection of the chains trace plots and also by estimating the autocorrelation time (Foreman-Mackey et al. 2013), resulting in ~150 steps on average for all parameters. From the 6×10^6 samples in the MCMC chain, we select as best fit model the maximum likelihood model, i.e. that with lowest normalised $\chi^2 \simeq 1$, as given by the following parameters: $I_0 = 10.72$ Jy sr^{-1}, $R_c = 0.46''$, $\gamma_1 = -0.39$, $\gamma_2 = 1.50$, $R_{g,1} = 0.12''$, $w_{1g,1} = 0.05''$, $w_{2g,1} = 0.01''$, $k_{1g,1} = 222.04$ arcsec^{-1}, $k_{2g,1} = 52.82$ arcsec^{-1}, $\delta_{g,1} = 0.98$, $R_{g,2} = 0.25''$, $w_{1g,2} = 0.29''$, $w_{2g,2} = 0.11''$, $k_{1g,2} = 95.08$ arcsec^{-1}, $k_{2g,2} = 59.77$ arcsec^{-1}, $\delta_{g,2} = 0.70$, $R_{g,3} = $

---

[1] https://github.com/mtazzari/galario.

[2] The visibility weights w_j are the theoretical estimates obtained by the CASA software package.
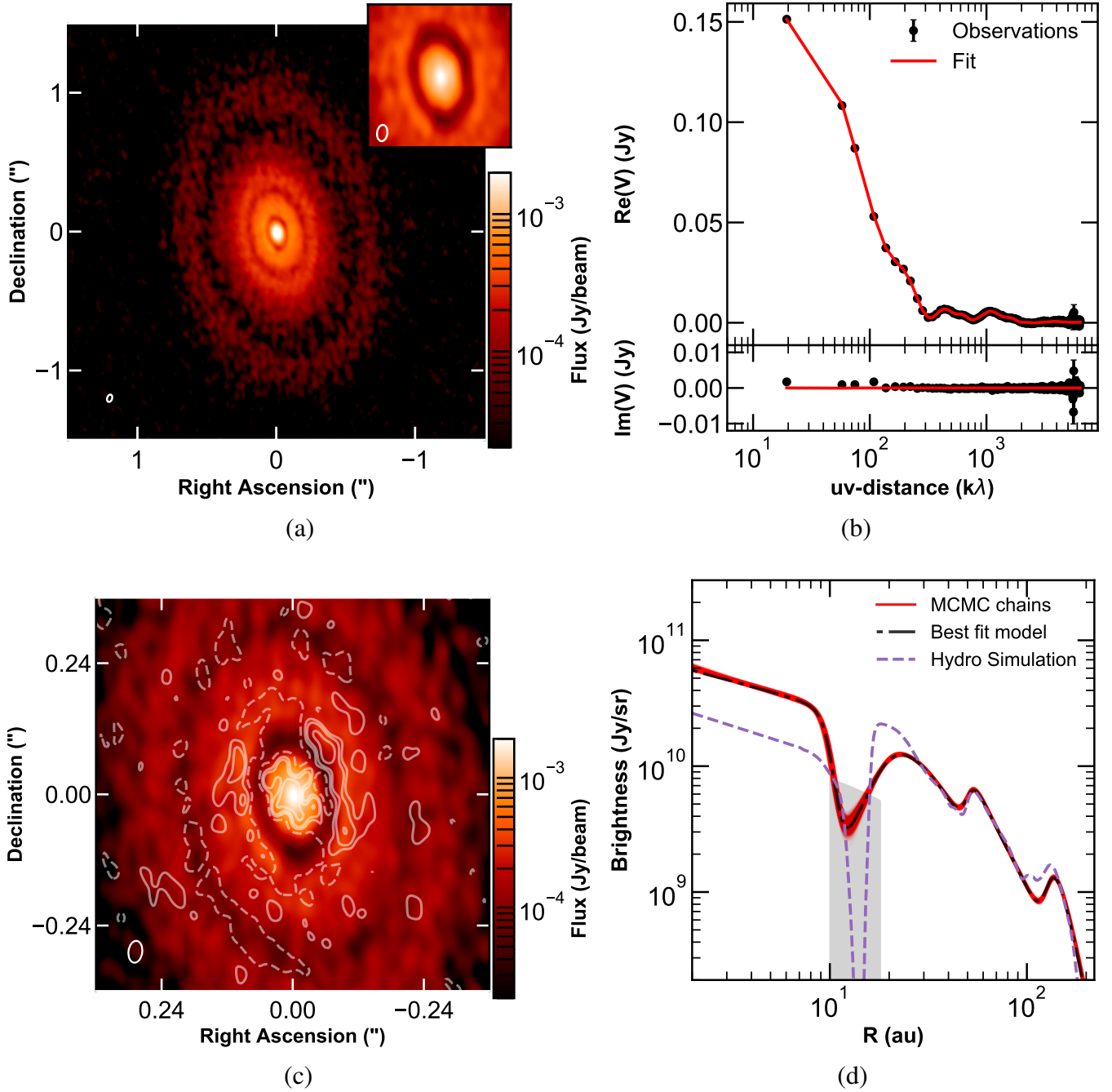
(a)

(b)

(c)

(d)

Figure 1. (a) Synthesized image of the CI Tau continuum observations (beam 50×30 mas FWHM, corresponding to 7×4 au). The rms noise level is $\sigma = 13\mu$Jy beam^{-1}. The inset shows a 0.35" wide zoom on the innermost gap imaged with a finer resolution (uniform weighting; 40×25 mas or 5×3.5 au, FWHM beam). (b) Observed visibilities compared with the best fit model visibilities as a function of deprojected baseline. (c) Synthesized image (uniform weighting) with fit residuals as white contours drawn at -3σ, 3σ, 6σ, 12σ, etc. (d) A family of 5×10^3 emissivity profiles drawn from the posterior (red). The black dot-dashed line highlights the best fit model. The gray shaded region indicates the range of gap depths that are still compatible with the observations. The dashed purple line shows the brightness profile obtained from the hydrodynamical simulation.

$0.88''$, $w_{1g,3} = 0.64''$, $w_{2g,3} = 0.06''$, $k_{1g,3} = 11.68 \, \mathrm{arcsec}^{-1}$, $k_{2g,3} = 21.87 \, \mathrm{arcsec}^{-1}$, $\delta_{g,3} = 0.84$, $R_{out} = 2.77''$, $i = 49.24°$, $PA = 11.28°$, $\Delta RA = 0.33''$, $\Delta Dec = -0.09''$. This maximum likelihood model falls in the central 68% interval of the posterior distribution of all parameters and indeed its brightness profile is representative of the density of models generated by the posterior (see panel (d) of Figure 1). In panel (b) of Figure 1 we compare the observed visibilities and those of the best fit model as a function of deprojected baseline. Panel (d) shows a family of 5×10^3 models drawn from the inferred posterior (red lines) and the best fit model (black dot dashed line): the brightness profile is tightly constrained between 20 and 100 au (i.e., the spatial scales probed by most of the interferometric baselines in the dataset) and more uncertain for $R < 20$ au. Thus we cannot firmly constrain the detailed shape of the innermost gap, whose width is comparable to the beam (~ 7 au). We explored in greater detail this degeneracy with a dedicated model suite and found an upper limit on the ratio of the flux inside to outside the gap of ~ 0.28: the gray shaded area in panel (d) highlights the range of brightness values that is compatible with the data.

The synthesized image of the residuals obtained for the best fit model is shown in panel (c) of Figure 1: there are virtually no residuals ($< 3\sigma$) in most of the disc at radii $R > 25$ au, confirming the axisymmetry of the brightness profile. The residuals are most significant (up to a 12σ level) at the disc center and in the North-West of the innermost ring. The central residuals reflect the fact that the functional form we have adopted is insufficiently flexible to correctly capture the emissivity profile in the innermost disc. The latter non-axisymmetric residuals might be caused by a combination of optical depth effects owing to the viewing angle of the observations ($i \sim 49°$) and a genuine difference in the local dust temperature.

We note that any perturbation of the disc caused by the hot-Jupiter at 0.1 au would occur on a scale of a few times its orbital radius and would thus be indistinguishable within the synthesized beam of 7×4 au.

4. MODELING THE EMISSIVITY PROFILE: EVIDENCE OF MULTIPLE PLANETS?

Structure in protoplanetary discs can derive from many causes. Non-planetary mechanisms proposed to date are however not well matched to CI Tau, e.g. photoevaporation produces holes rather than gaps (Ercolano et al. 2017), while simulations of the vertical shear instability (Flock et al. 2017) and of non-ideal MHD effects (Flock et al. 2015) do not produce the well spaced multiple rings seen in CI Tau. While gaps may also arise from opacity effects associated with ice sublimation fronts (Zhang et al. 2016), the outermost two rings are well outside the sublimation fronts of even the least volatile species, N_2 and CO (Kwon et al. 2015). Moreover,

in the innermost gap, our modelling implies a depletion of the optical depth by a factor ~ 50 compared with adjacent regions, considerably more than can be attributed to opacity variations. We therefore focus on the planetary hypothesis. While gap width can be used to infer the required planet mass (Rosotti et al. 2016), this conversion depends on the turbulence in the disc, as parameterised by the Shakura-Sunyaev α parameter (Shakura & Sunyaev 1973), which controls the transport properties of both dust and gas. The level of disc turbulence is difficult to constrain observationally: some estimates based on turbulent line broadening have suggested very low α values which then struggle to reproduce observed accretion rates (Flaherty et al. 2015) although the universality of this result has been questioned (e.g. Teague et al. 2016). We explore hydrodynamical models in which α and the gas surface density are constrained by the observed high accretion rate onto the star ($\dot{M} = 3 \times 10^{-8} M_\odot \, \mathrm{yr}^{-1}$ McClure et al. 2013), assuming this accretion to be driven by some form of turbulent viscosity; the highly axisymmetric image moreover implies that the disc is not self-gravitating. Together these constraints favour a rather high α value ($> 10^{-2}$). We also assume that the maximum grain size, a_{max} is locally determined by the minimum of two limits imposed by radial drift and fragmentation, assuming a fragmentation velocity of 10 m s^{-1} (Birnstiel et al. 2012). We compute the corresponding dust opacity (Tazzari et al. 2016) assuming a population of compact silicate grains with size distribution $dn/da \propto a^{-3}$ for $a < a_{max}$. and in our emissivity modeling adopt the temperature profile derived by Kwon et al. (2015). We assume an initial dust to gas ratio of 0.01.

Below we describe simulations of our fiducial model with parameters $\alpha = 0.014$ and total disc mass within 200 au of 20 M_{Jupiter}. These parameters imply strong accretion in the disc ($\sim 10^{-8} M_\odot \, \mathrm{yr}^{-1}$) and yield a profile of a_{max} that is compatible with measurements of the disc-averaged spectral index in CI Tau. [3] We use these parameters in hydrodynamical simulations where we insert three planets in the disc, using the 2D version of the FARGO3D code (Benítez-Llambay & Masset 2016) with our implementation of drag coupled dust (Rosotti et al. 2016). We employ 350 logarithmically spaced cells in the radial direction (from 5.6-378 au) and 512 cells azimuthally, producing approximately square cells at each location. We adopt an initial gas surface density profile $\Sigma_{gas} \propto 1/r$ normalised at 8 g cm^{-2} at 25 au, steepening to a $1/r^2$ profile beyond 60 au. The local value of a_{max} is computed as above. We then compute a synthetic emissivity profile (using the temperature profile and calculation of opacity as a function of a_{max} detailed above) for direct comparison with our GALARIO derived profile. The purple

---

[3] A spectral index of 2.9 ± 0.35 is derived by comparing our 1.3mm flux with the 2.7mm measurements of Guilloteau et al. (2011).
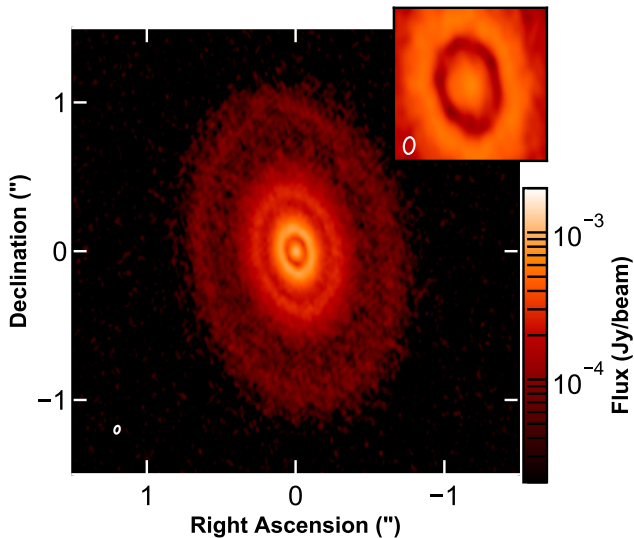
Figure 2. CLEANed image of the continuum emission obtained from our gas and dust hydrodynamical simulation containing three planets. This synthetic image was produced with the same noise level as in the observations and using the same imaging parameters used in Fig. 1.

dashed line in panel (d) of Figure 1 presents the brightness profile of our fiducial model where planets of mass 0.75, 0.15 and 0.4 M_{Jupiter} are located at orbital radii of 14, 43, and 108 au. We also produce a synthesized image (Fig. 2), generating model visibilities via the `ft` task in CASA with exactly the same uv-plane coverage and observational setup as the actual observations and then CLEANing the image using the same imaging parameters as the observed image. Note that for a given disc model, the planet mass within the innermost gap is only determined to within around a factor of two since this gap is poorly resolved, while the values are constrained to within around 30% in the outer two gaps.

5. DISCUSSION

5.1. *Observational tests of the fiducial model*

Our fiducial model is motivated by reproducing accretion rate and spectral index data for CI Tau, which results in moderately high turbulence levels ($\alpha \sim 0.01$). In HL Tau Pinte et al. (2016) have argued for low turbulence levels on account of the narrowness of the ring features; in CI Tau, however, the somewhat wider gaps and colder disc means that the turbulence levels cannot be constrained in this way. The ratio of total fluxes at 2.7 to 1.3 mm in fact *requires* that a_{max} in the outer, optically thin, regions of CI Tau is relatively low ($< 1\,\mathrm{mm}$), in agreement with our model. CI Tau may be relatively unusual in lacking larger grains (its mm spectral index lies at the $\sim$ 85th percentile among protoplanetary discs; Testi et al. 2014). An alternative scenario, if we put aside the evidence from the mm spectral index for small grains in

the outer disc, is that disc accretion is driven by a magnetised wind (e.g., Bai 2016). rather than turbulent viscosity. Low turbulence levels allow grains to grow and partially decouple from the flow so that lower planetary masses are required to match the observed gap parameters: from the hydrodynamical simulations of Rosotti et al. (2016) (where $\alpha = 10^{-3}$) we estimate planet masses of 20-30 earth masses for the outer two although a mass of up to around a Jupiter mass can be accommodated in the case of the innermost planet. Spatially resolved spectral index determinations (Tazzari et al. 2016) as well as searches for possible kinematic distortions expected from a gas giant planet (Pinte et al. 2018; Teague et al. 2018), could potentially discriminate between these possibilities.

5.2. *Evolutionary scenarios for the fiducial model: formation and migration*

The inferred planet masses in the three gaps suggest that none of these planets formed through gravitational instability. Planets formed in this way should exceed the Jeans limit in the outer disc (about a Jupiter mass) and should rapidly grow to much larger masses by accretion (Kratter & Lodato 2016). The hot Jupiter on the other hand could have been formed by a variety of mechanisms; from the modeled masses in disc and planets and from the accretion on to the star the inferred timescale for its inward migration is $\sim$ 0.4 Myr (Dürmann & Kley 2015) so that there would have been plenty of time for it to have migrated from a range of outward lying locations. The roughly Jovian mass planet inferred at 14 au is also easy to account for in terms of existing planet formation models (i.e. core accretion models involving either planetesimal or pebble accretion (Ida et al. 2013; Bitsch et al. 2015)). However neither of these models readily account for the two lower mass planets at 43 and 108 au. The timescales for forming and accumulating solid material are long in the outer disc (though see Rafikov 2011 for arguments in favour of planetesimal accretion at large orbital radii). Even if this were circumvented, these planets would have had to have grown through the mass range (10-20 earth masses) where rapid inward migration is expected (Paardekooper et al. 2011) and so their existence at large radii is a puzzle. Ida et al. (2013) were able to generate a modest population of gas giants at large separations through outward scattering of planetary cores and subsequent accretion but their population synthesis models only sparsely populate the parameter space corresponding to the two outer planets in CI Tau.

It is unclear whether the current planetary architecture would survive on Gyr timescales. The planets' period ratios do not suggest a resonant configuration. Nevertheless, the relatively high disc mass means that they may still end up at small radii, possibly being swallowed by the star or ejected from the system by scattering off the hot Jupiter (Lega et al. 2013). While current imaging surveys of mature systems do

not have the sensitivity to detect planets of the masses we infer in CI Tau (Vigan et al. 2017), future surveys will be able to determine if CI Tau-like systems are long lived.

5.3. *Comparison with other gapped discs*

High resolution ALMA studies are steadily increasing the census of discs with annular substructure. Although unique in being the only such system with a hot Jupiter, CI Tau's ring structure is not unusual. Its well spaced broad annuli place it in a similar category to HL Tau, HD 163296 and HD 169142 (ALMA Partnership et al. 2015; Isella et al. 2016; Fedele et al. 2017); none of the above systems exhibit the closely spaced shallow features seen in TW Hydra (Andrews et al. 2016) or the narrow deep features seen in AS 209 (Fedele et al. 2018). However only TW Hydra and HL Tau have been observed at a comparably high resolution to this study. Previous modeling of the gap structures in HL Tau (e.g. Dipierro et al. 2015) have yielded similar planet masses as a function of disc parameters to what we report here, although in HL Tau the choice of disc model has not been constrained by other system observables.

6. CONCLUSIONS

High resolution ALMA data of the disc in the young star CI Tau has revealed three prominent annular emission gaps which we have interpreted as an ensemble of massive planets spanning a factor thousand in orbital radius. The wealth of supplementary data available on CI Tau has allowed us to construct models that are consistent with *all* the data on this system available to date. The inferred planetary architecture suggests that the observed association between hot Jupiter and other companions may be in place at very early times. We note that the outer two planets (sub Jovian planets at radii of 43 and 108 au) present a challenge to current planet formation models.

Software: GALARIO v1.2 (Tazzari et al. 2018), emcee v2.2.0 (Foreman-Mackey et al. 2013), CASA v5.1.1 (McMullin et al. 2007).

REFERENCES

ALMA Partnership, Brogan, C. L., Pérez, L. M., et al. 2015, ApJL, 808, L3

Andrews, S. M., & Williams, J. P. 2007, ApJ, 659, 705

Andrews, S. M., Wilner, D. J., Zhu, Z., et al. 2016, ApJL, 820, L40

Bai, X.-N. 2016, ApJ, 821, 80

Becker, J. C., Vanderburg, A., Adams, F. C., Khain, T., & Bryan, M. 2017, AJ, 154, 230

Benítez-Llambay, P., & Masset, F. S. 2016, ApJS, 223, 11

Biddle, L. I., Johns-Krull, C. M., Llama, J., Prato, L., & Skiff, B. A. 2018, ApJL, 853, L34

Birnstiel, T., Klahr, H., & Ercolano, B. 2012, A&A, 539, A148

Bitsch, B., Lambrechts, M., & Johansen, A. 2015, A&A, 582, A112

Dipierro, G., Price, D., Laibe, G., et al. 2015, MNRAS, 453, L73

Dürmann, C., & Kley, W. 2015, A&A, 574, A52

Ercolano, B., Rosotti, G. P., Picogna, G., & Testi, L. 2017, MNRAS, 464, L95

Fedele, D., Carney, M., Hogerheijde, M. R., et al. 2017, A&A, 600, A72

Fedele, D., Tazzari, M., Booth, R., et al. 2018, A&A, 610, A24

Flaherty, K. M., Hughes, A. M., Rosenfeld, K. A., et al. 2015, ApJ, 813, 99

Flock, M., Nelson, R. P., Turner, N. J., et al. 2017, ApJ, 850, 131

Flock, M., Ruge, J. P., Dzyurkevich, N., et al. 2015, A&A, 574, A68

Foreman-Mackey, D., Hogg, D. W., Lang, D., & Goodman, J. 2013, PASP, 125, 306

Guilloteau, S., Dutrey, A., Piétu, V., & Boehler, Y. 2011, A&A, 529, A105

Guilloteau, S., Simon, M., Piétu, V., et al. 2014, A&A, 567, A117

Haisch, Jr., K. E., Lada, E. A., & Lada, C. J. 2001, ApJL, 553, L153

Ida, S., Lin, D. N. C., & Nagasawa, M. 2013, ApJ, 775, 42

Isella, A., Guidi, G., Testi, L., et al. 2016, Phys. Rev. Lett., 117, 251101

Johns-Krull, C. M., McLane, J. N., Prato, L., et al. 2016, ApJ, 826, 206

Kley, W., & Nelson, R. P. 2012, ARA&A, 50, 211

Knutson, H. A., Fulton, B. J., Montet, B. T., et al. 2014, ApJ, 785, 126

Konishi, M., Hashimoto, J., & Hori, Y. 2018, ApJL, 859, L28

Kratter, K., & Lodato, G. 2016, ARA&A, 54, 271

Kwon, W., Looney, L. W., Mundy, L. G., & Welch, W. J. 2015, ApJ, 808, 102

Lega, E., Morbidelli, A., & Nesvorný, D. 2013, MNRAS, 431, 3494

Mayor, M., & Queloz, D. 1995, Nature, 378, 355

McClure, M. K., Calvet, N., Espaillat, C., et al. 2013, ApJ, 769, 73

McMullin, J. P., Waters, B., Schiebel, D., Young, W., & Golap, K. 2007, in Astronomical Society of the Pacific Conference Series, Vol. 376, Astronomical Data Analysis Software and Systems XVI, ed. R. A. Shaw, F. Hill, & D. J. Bell, 127

Ngo, H., Knutson, H. A., Hinkley, S., et al. 2015, ApJ, 800, 138

Paardekooper, S.-J., Baruteau, C., & Kley, W. 2011, MNRAS, 410, 293

Pinte, C., Dent, W. R. F., Ménard, F., et al. 2016, ApJ, 816, 25

Pinte, C., Price, D. J., Ménard, F., et al. 2018, ApJL, 860, L13

Rafikov, R. R. 2011, ApJ, 727, 86

Rasio, F. A., & Ford, E. B. 1996, Science, 274, 954

Rosotti, G. P., Juhasz, A., Booth, R. A., & Clarke, C. J. 2016, MNRAS, 459, 2790

Shakura, N. I., & Sunyaev, R. A. 1973, A&A, 24, 337

Simon, M., Guilloteau, S., Di Folco, E., et al. 2017, ApJ, 844, 158

Tazzari, M., Beaujean, F., & Testi, L. 2018, MNRAS, 476, 4527

Tazzari, M., Testi, L., Ercolano, B., et al. 2016, A&A, 588, A53

Teague, R., Bae, J., Bergin, E. A., Birnstiel, T., & Foreman-Mackey, D. 2018, ApJL, 860, L12

Teague, R., Guilloteau, S., Semenov, D., et al. 2016, A&A, 592, A49

Testi, L., Birnstiel, T., Ricci, L., et al. 2014, Protostars and Planets VI, 339

Vigan, A., Bonavita, M., Biller, B., et al. 2017, A&A, 603, A3

Wright, J. T., Marcy, G. W., Howard, A. W., et al. 2012, ApJ, 753, 160

Zhang, K., Bergin, E. A., Blake, G. A., et al. 2016, ApJL, 818, L16